UCRL-JC-125397
PREPRINT

Penetrating Radiation Impact on NIF Final Optic Components

C. D. Marshall
J. A. Speth
L. D. DeeLoach
S. A. Payne

This paper was prepared for submittal to the
Solid-State Lasers for Application to Inertial Confinement Fusion Conference
Paris, France
October 22-25, 1996

October 15, 1996

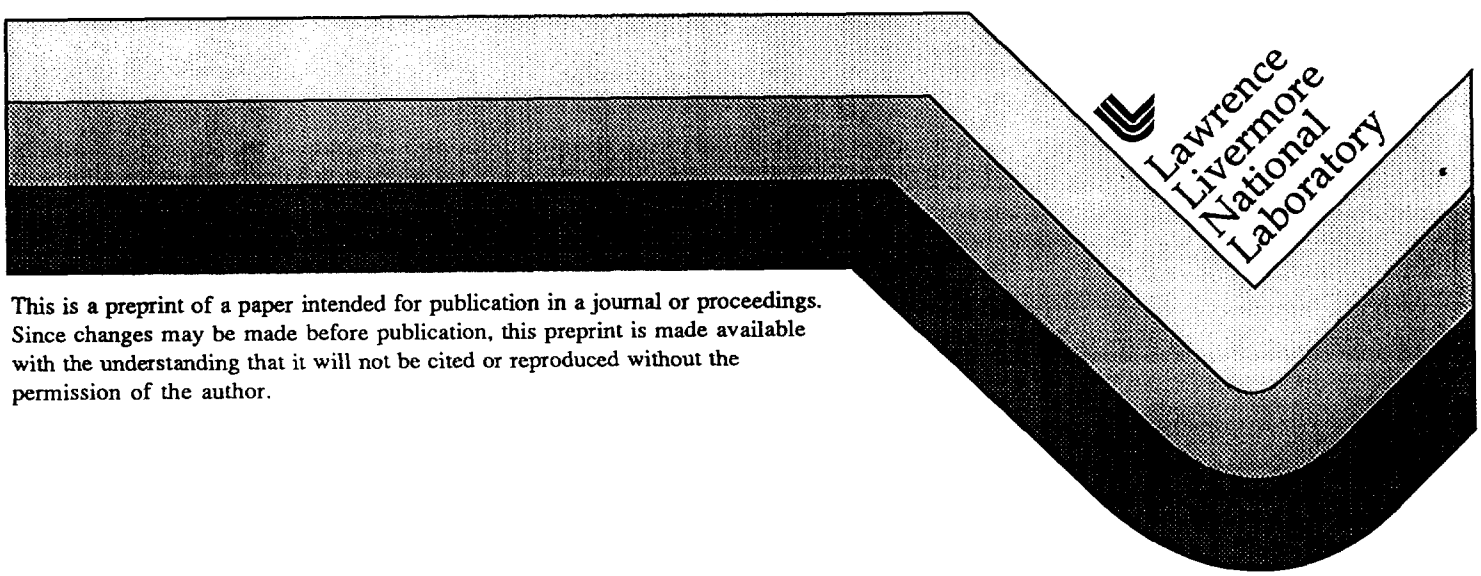

Penetrating radiation impact on NIF final optic components

C. D. Marshall, J. A. Speth, L. D. DeLoach, and S. A. Payne

Lawrence Livermore National Laboratory,
P. O. Box 808, Livermore, CA 94550

ABSTRACT

The principal technical goal of the National Ignition Facility (NIF) is to achieve thermonuclear ignition in a laboratory environment via inertial confinement fusion (ICF). This will enable NIF to service the DOE stockpile stewardship management program (SSMP), inertial fusion energy goals, and advance scientific frontiers.[1] All of these applications will make use of the extreme conditions that the facility will create in the target chamber. In the case of a projected 20 MJ yield scenario, NIF will produce ~10^{19} neutrons with a characteristic DT fusion 14 MeV energy per neutron. There will also be a substantial amount of high energy x-rays as well as solid, liquid and gaseous target debris produced either directly of indirectly by the inertial confinement fusion process. A critical design issue is the protection of the final optical components as well as sophisticated target diagnostics in such a harsh environment.

Keywords: Radiation effects, optical materials, National Ignition Facility, Inertial Confinement Fusion.

I. Introduction

Figure 1 shows the basic geometry of the NIF target chamber where the final optic package is located 6.5 m from the target and chamber center. The debris shields are designed to absorb the x-rays and target debris and will likely require frequent replacement. The target chamber wall and ~1 m thick concrete shielding as well as the target area concrete shield wall (not shown in Fig. 1) will absorb virtually all of the radiation and target debris and will protect the majority of the laser system from direct line of sight irradiation. Penetrating radiation such as neutrons and gamma-rays, however, will propagate through the ~1 cm thick debris shields to interact with the relatively expensive fused silica focus lenses and KDP frequency conversion crystals. This article will focus on the potential degradation of the final focus lenses and frequency conversion crystals for NIF that are needed to last for many years. Furthermore, an ICF-based power plant may become possible in the next century, when it will likely be necessary to hold the SiO_2 final optic at an elevated temperature in order to rapidly anneal out the radiation induced defects that are formed.[2]

Fused silica (synthetic SiO_2) or fused quartz (natural SiO_2) have long been considered to be among the optical materials of choice for situations involving ultraviolet transparency, precision quality, large size, or harsh environmental conditions. The issues surrounding the radiation-hardness of SiO_2 have been studied for many decades now,[3,4,5,6] and the recent emergence of deep-ultraviolet (DUV) lithography has prompted a renewed interest.[7,8,9] Many defects have been successfully characterized and elucidated, and this report builds on this foundation,[3,4,5,6] however, substantial uncertainty still pervades the literature. This situation is partly a consequence of the often unclearly specified radiation conditions and the different types of SiO_2 that were used. Here we report the results of testing on a wide variety of commercial fused silica and quartz samples, with a wide variety of specified irradiation conditions, leading to an improved understanding of the issues important for SiO_2 radiation-hardness with a particular emphasis on application to ICF.

Far less is known about the radiation resistance of KDP.[10,11] The work described below is intended to assess the radiation-hardness and unravel some of the basic material physics associated with SiO_2 and KDP that have encountered γ-ray, or neutron irradiation.[12]

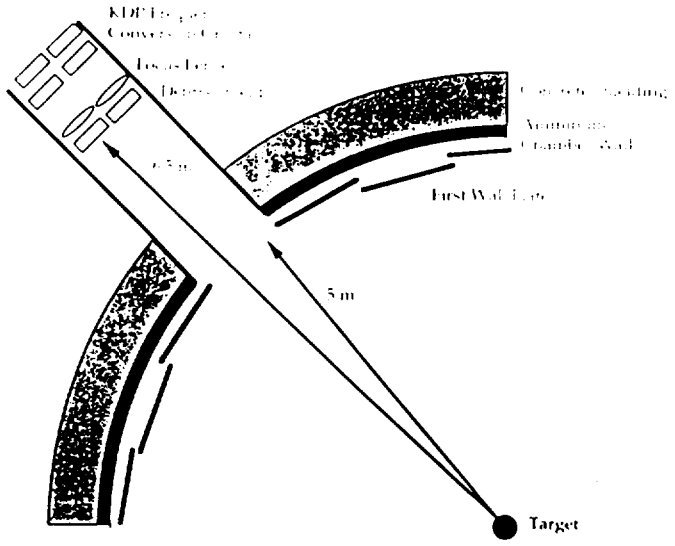

Figure 1. Geometry of the NIF target chamber showing the position of the final optical components.

In general when electromagnetic radiation of sufficient energy is utilized to irradiate an optical material, solarization or optical darkening, occurs. Absorption or scattering of photons leads to the generation of energetic electrons and holes which eventually react with pre-existing structural defects (precursors) or the intrinsic material itself to create the electronic defects associated with solarization.[5,13]

A ~1 MeV γ-ray, typical of the energy range to be produced on NIF from secondary neutron reactions, is, in principle, capable of yielding about 10^5 e-h pairs per photon. The process begins by the production of energetic Compton electrons, which subsequently produce secondary electrons and e-h pairs. The action of neutrons is quite different than γ-ray photons, due to their uncharged nature. Neutrons initially collide with nuclei, and can induce nuclear reactions which produce other types of radiation such as gamma rays, alpha particles etc., however, it always imparts some amount of momentum transfer. The resulting "knock-on-collision" displacement damage can lead to precursor sites that later encounter the electrons and holes and become converted to other types of defects. Precursors can also result from the manufacturing processes, such as from oxidizing or reducing conditions.

Many different defects can be created in SiO_2 and KDP materials from irradiation. The following description outlines those most prominently observed in our studies. Perfect SiO_2 glass is comprised of silicon tetrahedrally bonded by four oxygens in a continuous random glass network. The Si-O-Si bonds can be strained, which is believed to render the site to be more susceptible to electronically-induced displacements.[14] An oxygen deficient center (ODC), which gives rise to an absorption band at 5 eV can be created as a result of collisions with neutrons.[15] The ODC can be converted to an E' defect center by losing an electron;[5,16,17] the E' absorption occurs at 5.8 eV. The precise absorption spectra associated with all defect species has not yet been fully resolved. For example, the B_1 with an absorption at 4 eV is only observed in fused quartz and a definitive defect site has not been correlated with this band.[5,15] An Al impurity[15,18] is known to give rise to absorption at 2.0 eV while a Ge impurity creates an absorption

at 5 eV (241 nm). We have found evidence of the Al and Ge impurity induced absorption, B_1, D_0, and E absorption bands in the course of this work.

Many different absorption bands have been identified with impurities and γ-ray irradiation in KDP. For example, transition metals such as Al, Fe, As, Cr, Pb, and V, can lead to significant radiation induced absorption in KDP, all with absorptions in various portions of the ultraviolet spectrum. In general, these absorptions are due to electrons that are promoted to the KDP conduction band via irradiation in similar ways to that described above for SiO_2. The electrons are then trapped at impurity sites in the band gap between the conduction and valence band. The energy gap between the impurity site and the conduction band lower edge determines the wavelength of the induced absorption.

II. Penetrating radiation characteristics

A. NIF

Although the majority of the penetrating radiation emanating directly from the target is 14 MeV monochromatic neutrons (17.6 MeV DT fusion γ-rays are down by 10^4 in flux), there are a significant number of neutron induced nuclear reactions with various structures in the target area as previously described by Latkowski and Tobin.[19] These secondary reactions produce penetrating radiation consisting of neutrons that range from <<0.01 MeV to ~10 MeV in energy and γ-rays ranging from 0.01 to 10 MeV. Depending on whether the radiation is prompt (directly from the target) or secondary radiation, the pulse duration is in the range of 5 to 100 ns, respectively.

The time integrated dose over an expected 30 year lifetime of NIF is expected to be 1.1 Mrad from neutrons (n^o) and 0.6 MRads from γ-rays in the SiO_2 focus lenses, and 1.1 Mrad n^o and 0.5 γ-rays in KDP. This corresponds to ~2 and ~1 kRads, of n^o and γ-rays respectively, for each of the 20 MJ yield shots with a total 385 MJ/year yield,[19] where 1 Rad is conventionally defined to be 10^{-5} Joules of absorbed energy per gram of material. There are of course variations in both the transverse and longitudinal directions relative to the beam tube or final optic package central axis due to absorption and shadowing, but the ±~10% variation is not significant compared to other issues such as the NIF gain and shot rate which may be accelerated.

B. Radiation testing sources

There are no radiation test sources currently operating that produce such a spectrum of neutrons and gamma rays with sufficient dose to be meaningful for accelerated life tests of the NIF final optics. As a consequence we have utilized a variety of radiation sources that bracket the problem to allow us to interpolate the results to predict what will happen on NIF. Table I gives a complete list of the radiation sources that have been utilized. The relevant temporal and spectral characteristics of the radiation sources are summarized. Modeling exercises benchmarked against the accumulated data, has provided a realistic view of what may be expected from the NIF. A brief description of each radiation source utilized for these studies follows.

The Los Alamos Neutron Science Center (LANSCE) is a 1 km long proton-accelerator neutron-spallation source that provides hard neutron and γ-ray spectrum extending from thermal energies <<0.01 MeV up to several hundred MeV. The pulse format of the accelerator furnishes a long (ms) train of 300-ps pulses with a macro repetition rate of 10 Hz. This facility allowed us to obtain both neutron and γ-ray irradiations with energies and doses that spanned the NIF relevant range.

The Sandia National Laboratory pulsed reactor facility No. III (SPR-III) is an enriched ^{235}U pulsed nuclear reactor that provides a relatively hard (for a reactor) neutron spectrum extending from thermal energies to ~3 MeV.[20] The reactor was nominally operated with 100 μs pulses at a repetition rate of once every 2 hours. The neutron energy spectrum is peaked at 1 MeV but is broad with 99% of the neutron energy bracket within 0.01 to 10 MeV. A high energy cutoff above 3 MeV is where the flux ($n/cm^2/MeV$) is down by an order of magnitude from the peak. This facility allowed us to obtain γ-ray irradiations with

energies that were close to the NIF relevant range, along with n° irradiation with energies near that of NIF (see Table I).

The French Commissariat Energie Atomique (CEA) Sames neutron source and LLNL RTNS-II neutron source are D accelerators with T targets that provided a continuous source of direct 14 MeV DT fusion neutrons. These facilities provided us with the best match to the neutron energies on NIF but the continuous temporal format is dissimilar. Gamma ray irradiation is also present in these sources due to secondary reactions.

An electron accelerator spallation source at LLNL and a ^{60}Co source also provide pure γ-ray radiation in ns pulsed and continuous formats, respectively, and 0.01-50 and 1 MeV energies, respectively. These γ-ray facilities, in conjunction with the mixed neutron and γ-ray sources, described above allowed for the separation of effects that arose from γ-rays and neutrons.

Table I: Summary of radiation source characteristics that were collaboratively utilized for accelerated life testing of NIF final optics components at Los Alamos National Laboratory (LANL), Sandia National Laboratory (SNL), Lawrence Livermore National Laboratory (LLNL), and several French Commissariat Energie Atomique (CEA) Laboratories

		NIF	LANL LANSCE	SNL SPR-III	LLNL RTNS-II	CEA Sames	LLNL ^{60}Co	LLNL e⁻ LINAC
Neutrons	Spectra (MeV)	14 primary <0.01-1 low dose	<0.01-100	<0.01-1	14	14	None	None
	Pulse format	5 ns	ps trains	100 μs	continuous	continuous (or 5 ns)	-	-
	CDR 30 yr. Dose (MRads)	1	✔	✔	✔	X	X	X
γ-rays	Spectra (MeV)	0.01 - 10	1-100	0.01 - 1	0.01 to 1	0.01 to 1	1	0.01-50
	Pulse format	20 ns	ps trains	100 μs	continuous	continuous	continuous	20 ns
	CDR 30 yr. Dose (MRads)	0.5	✔	✔	X	X	✔	✔

III. Experiments

Using the information described below on experiments performed with the radiation sources listed in Table I, we have developed a physical model of the primary radiation damage pathways for silica glass and KDP in the penetrating radiation dose range of interest for NIF. Experiments were conducted on all of the penetrating radiation sources described above. The primary consideration was the induced optical absorption in the glasses as a function of the absorbed radiation dose. The temporal format of the radiation pulses was also of interest as there is potential thermal annealing at room temperature that could effect radiation damage of subsequent pulses. The radiation spectral shape was also of concern as different energy neutrons have differing percentages of elastic and inelastic scattering. We studied as many as 25 sources and grades of SiO_2 to understand the impact of manufacturing methods on precursors to damage. In addition we studied many different impurities deliberately doped in KDP in order to understand the impact of starting material purity and process control as described below in Section III B.

A. Silica glass radiation effects

The wide variation in resistance from different glass manufacturing sources and processes is shown in Fig. 2, where eight type of SiO_2 were irradiated. Samples included fused quartz and fused silica with varying in manufacturing methods from many different vendors. All samples were simultaneously irradiated with identical 3.7 MRads of γ-rays from a ^{60}Co source. Despite their wide variation in radiation resistance, however, these samples led to only the four radiation induced absorption spectral shapes shown in Fig. 3. From this information and data obtained on other radiation sources it was possible to determine the origin of the prominent spectral shapes. The peak at 246 nm was determined to arise from direct-neutron collision-induced displacements creating a localized oxygen deficient center (ODC) that is intrinsic to all SiO_2. The absorption peak at 300 nm in Fig. 3b arises from the conversion of 241 nm defect absorption, that is present prior to irradiation, which is likely due to a Ge impurity color center as discussed below. The peak at 210 nm (E' defect) is due to a two step process of first creating the 246 nm ODC defect and then with converting into a E' center with γ-rays. The peak centered at 550 nm is likely due to Al impurities in the SiO_2, as suggested in the literature.[5,16,17] The four spectra shown in Fig. 3 correspond to four classes of SiO_2 noted in Table II. The most radiation hard variants are synthetic fused silicas such as Corning 7980 and Heraeus Suprasil grades.[12]

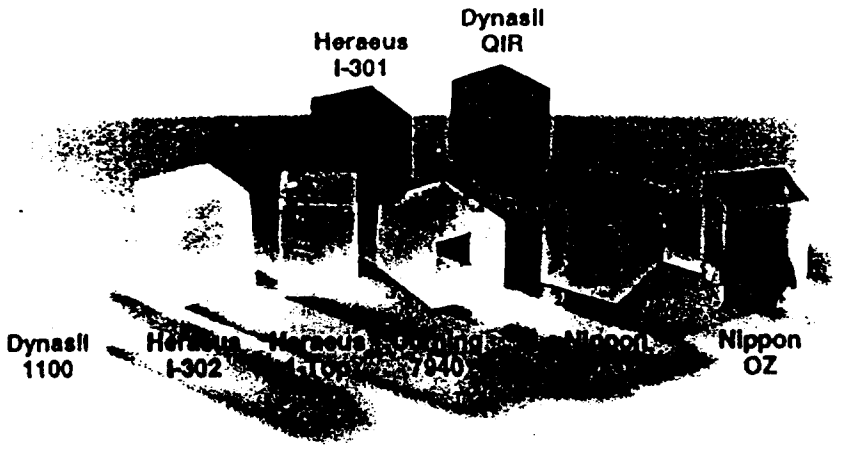

Figure 2. Eight different types of fused silica and fused quartz from several different manufacturers all irradiated with the same 3.7 MRads of γ-rays from a ^{60}Co source.

In an effort to benchmark the effective lifetime of the NIF optics we found that it was necessary to utilize a mixed neutron and gamma-ray source, since there are synergistic neutron and gamma pathways that lead to radiation induced damage. The SPR-III reactor proved to be a versatile radiation source for our purposes, with a 100 μs pulse operation, a mixed neutron and gamma dose ratio that is similar to NIF (within a factor of 5), and a gamma spectrum that is very close to that of NIF (see Table I). The neutron spectrum from this largely unmoderated U_{238} fission reactor, however, extends over a broad energy range as discussed above with a peak flux at 1 MeV. This is low when compared to the direct DT 14 MeV neutrons that will dominate the NIF spectrum. As a consequence these results must be extrapolated to higher neutron energies (more damage per individual collision cascade created by a single neutron) for making NIF predictions as is discussed below. The SPR-III data is intended to provide insight into the

Table II. All of the SiO2 sample types studied fell into four groupings of radiation response designated as FS1, FS2, FQ1, and FQ2, where FS = synthetic fused silica, and FQ = natural fused quartz

FS1 Synthetic Fused Silica "Rad-hard-type"	FS2 Synthetic Fused Silica "Rad-soft-type"	FQ1 Natural Fused Quartz "Rad-hard-type"	FQ2 Natural Fused Quartz "Rad-soft-type"
Corning 7980	Dynasil 1100	Heraeus Herasil-1top	Heraeus Infrasil-301
Corning 7940	Dynasil 1101	Heraeus Herasil-1	Dynasil QIR
Heraeus Suprasil-1		Heraeus Herasil-2	Nippon OZ
Heraeus Suprasil-2		Heraeus Herasil-3	Nippon OX1
Heraeus Suprasil-3		Heraeus Homosil	
Dynasil 4100		Heraeus Infrasil-302	
Dynasil 4101		Heraeus TO8	
Nippon ES		Dynasil QUV	
		Nippon OY	

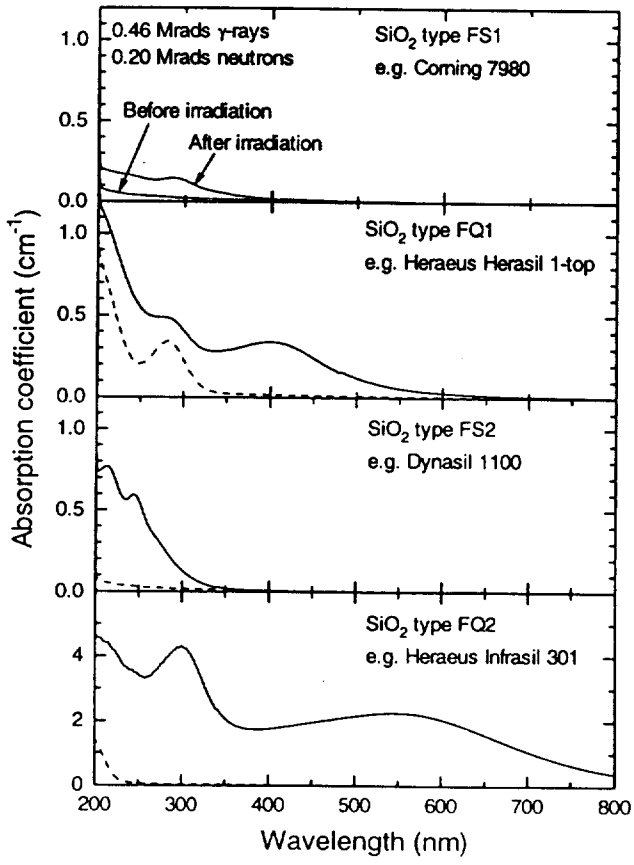

Figure 3. Under identical 200 krads neutron and 460 krads gamma irradiation doses, the absorption spectra of all 25 types of SiO_2 studied fell into the four distinct classes illustrated in parts (a), (b), (c), and (d)impact of the γ-ray/n^0 mix of radiation.

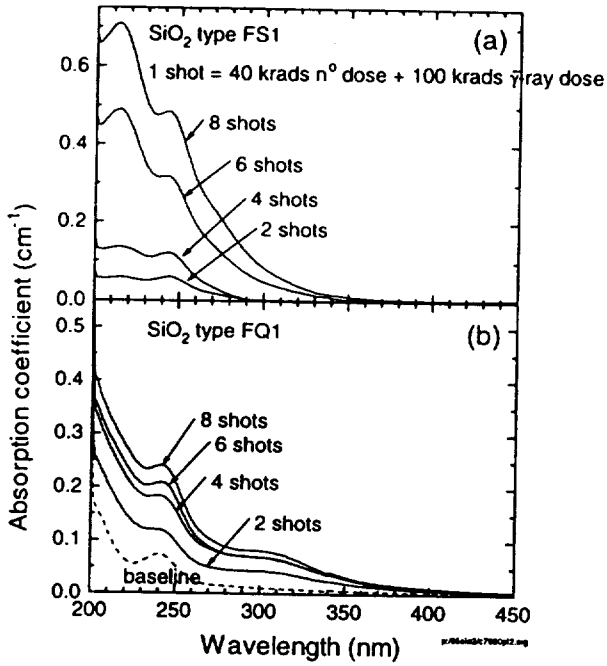

Figure 4. Optical absorption spectra of fused silica (a) and fused quartz (b) taken after successive shots on the SNL pulsed nuclear reactor number III. One shot has 40 krads n° and 100 krads γ-ray dose.

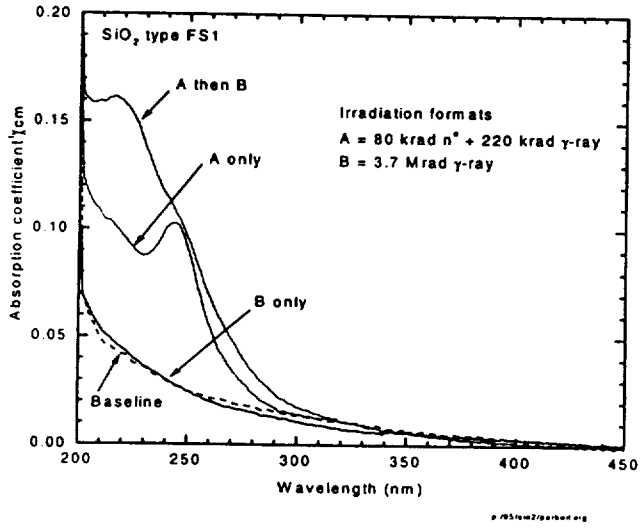

Figure 5. Optical absorption spectra of FS1 glass revealing that the oxygen deficient center created by neutrons can be converted to E' center absorption at 213 nm with γ-rays.

Figure 4 shows the results of performing a dose dependent study on SPR-III over the course of two experimental days. In one year on NIF with 385 MJ of fusion yield assumed in the NIF conceptual design report (CDR), NIF is predicted to produce ~40 krads of neutron dose and ~20 krads of γ-ray dose, hereafter referred to as a "NIF year". Note that one shot on SPR-III corresponds to one NIF neutron year and 5 NIF γ-ray years.

In Fig.4a the cumulative effect of up to 8 pulses from SPR-III is shown for the FS1 glasses, revealing that absorptions at 213 nm and 246 nm are both produced. Upon closer inspection, it is noticed that the E' center at 213 nm grows at an accelerated rate compared to the 246 nm feature. This observation suggests that neutrons first create the ODCs, which are then converted to E' centers by the γ-rays. A critical test to confirm this synergistic γ-ray/n^0 effect is shown in Fig. 5. Here the FS1-type sample is first irradiated in SPR-III to create the ODCs and then in a separate irradiation, subjected to pure γ-rays from the ^{60}Co source to show that the ODCs are converted to E' centers. It is important to recall that irradiation by γ-rays alone has no effect; i.e., the neutrons first "soften" the material by generating ODCs. We also observed that in fused quartz the 241 nm band, whose strength can be correlated to Ge concentration, is converted into a B1 center at 300 nm as shown in Fig. 4b. These above mechanisms are summarized in Fig. 6.

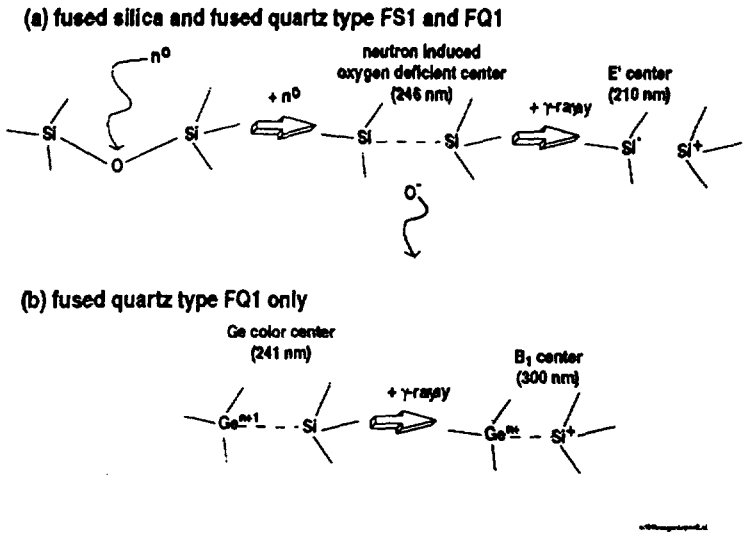

Figure 6. Mechanistic model of primary radiation damage mechanisms in SiO_2 that lead to changes in optical transmission. Note that both neutrons and γ-rays, either separately or in combination, can lead to radiation induced damage.

When using a pulsed radiation source, there is generally annealing of the induced defects following the radiation pulse; i.e., some of the defects are self healing at room temperature with relaxation times (inverse rate constants) ranging from ns to hours. The defects discussed in this paper are primarily long-lived defects that show no further decay after many days to months following irradiation at room temperature. The temporal format of the radiation pulse could in general affect the number of "permanent" defects observed, since annealable defects could be further affected by a subsequent radiation burst before they had a chance to decay. To test this possibility (i.e. explore the dose-*rate* dependence), we performed an experiment on the SPR-III reactor, where the radiation dose rate was varied over eight orders of magnitude. The results of this experiment are summarized in Fig. 7.

In the first experiment shown on the top of Fig. 7a the reactor was run in a steady state mode for 30 minutes with relatively low radiation flux. In the second experiment on the bottom of Fig. 7a, a 100 μs pulsed neutron format was utilized. The total time-integrated neutron (and γ-ray) dose during the 30 minute runs and the 100 μs pulses was measured to be approximately the same (to within 10% of $1.5x10^{15}$

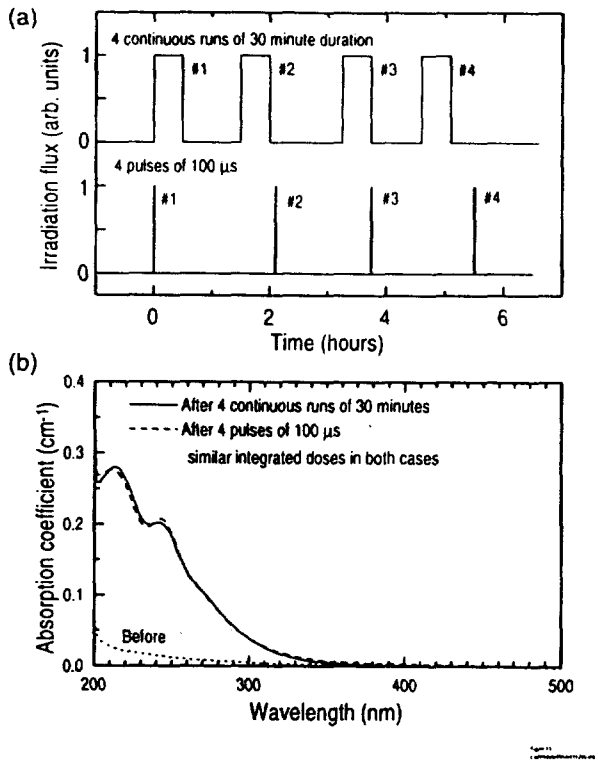

Figure 7. Experiment to study the effect of room temperature annealing with short pulse versus continuous irradiation. Part (a) temporal format of radiation flux from SPR-III nuclear reactor used in the experiments shown in part (b). Similar time integrated doses were utilized in both experiments.

n./cm^2. The neutron and γ-ray spectra are virtually identical for these two experiments, since the reactor has the same degree of moderation inside the core region. Care was taken to have the same overall experimental time elapse between pulses to have the best control possible.

The results of this analysis is given in Fig.7b with solid and dashed curves for continuous and pulsed formats, respectively. There is little dose rate dependency to the data over the range studied in this experiment. This can be rationalized by showing that the number density of defect centers is much less than the number density of atoms by four orders of magnitude. Consequently, one would expect that multiple collisions and interactions on a single physical site would be infrequent (i.e. 2 neutrons striking the same nucleus or damaged region) and that the system behaves as if single isolated collisional impact sites are present.

Figure 8 presents a reduction of the data in Fig. 4 which resulted from exposing (a) fused silica and (b) fused quartz with up to eight shots on the SPR-III reactor. The data in Fig. 4 were fit to a sum of Lorentzians, L(λ), to account for the absorption arising from each species:

$$\alpha_i(\lambda) = \sum_i \alpha_i N_i L_i(\lambda), \tag{1}$$

where

$$L_i(\lambda) = \frac{\Delta\lambda_i^2}{1+(\lambda_i - \lambda_n)^2} \tag{2}$$

is the peak wavelength and $\Delta\lambda$ is the half width at half maximum of the absorption spectrum for i = E', ODC or B_1. The open points in Fig. 8 gives the peak defect absorptions coefficients obtained from the Lorentzian curve fits to the spectra in Fig. 4. Note that with fused silica (part a), the absorption peak at 246 nm grows most rapidly at first and at higher doses the 210 nm absorption peak growth rate overtakes it. This qualitative observation is consistent with the model described by Fig. 6.

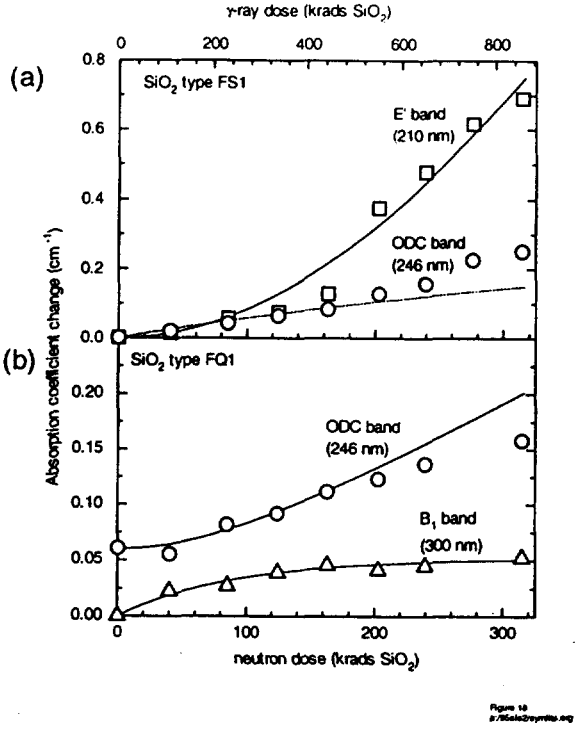

Figure 8. Radiation induced absorption of E'(210 nm), ODC (246 nm), and B1 (300 nm) bands in SiO_2 for fused silica type FS1 and fused quartz type FQ1 in parts (a) and (b), respectively. Data denoted as open symbols was obtained from SNL pulsed nuclear reactor experiments. The numerical modeling using Eqs. 1-3 is denoted as solid lines.

Quantitative modeling of the defect absorption peaks shown in Fig. 8a for fused silica can be performed by applying rate equations derived from the model in Fig. 6a for the number density of neutron induced ODC and subsequent γ-ray induced E' defects, denoted as N_{ODC_n} and $N_{E'}$, respectively. The rate equations can be written as:

$$\frac{dN_{ODC_n}}{dt} = M_{col}\sigma_{col}(E)N_{SiO_2}\frac{dF_n}{dt} - \beta_{E'}\frac{dD_\gamma}{dt}N_{ODC_n}, \text{ and} \quad (3)$$

$$\frac{dN_{E'}}{dt} = \beta_{E'}\frac{dD_\gamma}{dt}N_{ODC_n}. \quad (4)$$

The first term in Eq. 3 describes the formation of ODC defects due to direct neutron collisions, where F_n is the neutron fluence, σ_{col} is the neutron collision cross section, N_{SiO2} is the silica number density, and M_{col} is a collision multiplier that denotes the number of cascade collision induced defects due to a single primary neutron collision as shown in the first step of Fig. 4a. Equation 4 and the last term in Eq. 3 account for the second step in Fig. 6a where ODC defects are transformed into E' defects with γ-rays with a phenomenological conversion coefficient denoted β_{i}, and D_γ is the γ-ray dose in krads. Defect optical

absorption cross sections (σ_{ODC} and σ_i) are then multiplied by the number densities obtained from Eqs. 3 and 4.

For the modeling of the defect absorption peaks in fused quartz shown in Fig. 10b, the direct conversion of pre-existing Ge color centers absorbing at 241 nm into B1 defects, with number densities N_{ODC} and N_{B1} respectively can be written as:

$$\frac{dN_{B1}}{dt} = -\frac{dN_{Ge}}{dt} = \beta_{B1}\frac{dD_\gamma}{dt}N_{Ge} \qquad (5)$$

where β_{B1} is the gamma ray conversion coefficient. There is a non-zero initial condition for the Ge defect concentration determined from absorption spectra of the individual samples. The solid lines are fits generated from Eqs. 1-5. The parameters obtained from these curve fits are given in Table III. The five data fitting parameters lead to are overdetermined system as may not be evident from first glance at Table III. To first order, the two unknown optical cross sections, σ_i, and the neutron multiplier, M_n, determine the height of the four curves, while the two conversion coefficients, β_i, determine the shape of the data curves.

Table III. Parameter utilized to model data from SPR-III reactor Figs. 5-8 and to predict NIF fused silica final optics performance in Fig. 10.

Parameter	Value	Units	Source
Neutron absorption coefficient, $N_{SiO_2}\sigma_{cal}$	0.35	cm^{-1}	literature
ODC to E' γ-ray conversion coefficient, $\beta_{E'}$	0.0007	s/krads	data fit
Collision multiplier for 1 MeV neutrons, M_n	105	unitless	data fit
Collision multiplier for 14 MeV neutrons, M_n	200	unitless	data fit
Ge to B1 γ-ray conversion coefficient, β_{B1}	0.004	s/krad	data fit
Optical cross section for ODC defect, σ_{ODC}	2.1e-18	cm^2	data fit
Optical cross section for E' defect, $\sigma_{E'}$	3.2e-17	cm^2	literature
Optical cross section for B1 defect, σ_{B1}	1.8e-18	cm^2	data fit

On the basis of this interpretation, the collision multiplier can be estimated by way of the Kinchin-Pease expression[21]

$$M_n = \frac{0.8\,E_{dam}}{2E_{def}} \cdot \eta_{anneal} \qquad (6)$$

where E_{dam} is the average kinetic energy of the atom which receives the initial direct collision, given as[22]

$$E_{dam} = E_n \cdot \frac{2}{A + 2/3} \qquad (7)$$

for which A is the atomic mass (average of Si and two O), and E_n ~ 1 MeV is the neutron energy — yielding E_{dam} ~ 0.1 MeV. E_{def} is the defect formation energy of the ODC, which we estimate as 40 eV from calculations of SiC, a related covalently bound material.[23] η_{anneal} is an additional factor included by Diaz de la Rubia and others to account for the rapid annealing (< 1 ns) that occurs from the enormous local energy deposition following a neutron-nucleus collision. Estimates from simulations place η_{anneal}

~ 0.2 for fast neutrons.[21,24] Substitution into Eq. 9 yields M_n ~200, a value that is reasonably close to our experimental assessment of 105 given the level of approximation surrounding Eqs. 6 and 7.

In order to apply this model to NIF like conditions, the neutron multiplier obtained at 1 MeV average neutron energy must be extrapolated to 14 MeV for DT fusion neutrons that will be present on NIF. To facilitate this extension several experiments were analyzed from three different high energy neutron sources. Two experiments were performed on 14 MeV DT fusion neutron sources (CEA Sames and LLNL RTNS-II) and one set of experiments was performed on LANL LANSCE high energy > 100 MeV proton spallation neutron source.

Figure 9 shows the results of irradiating type FS1 fused silica (e.g. Corning 7980) with $2x10^{14}$ n/cm^2 in the Sames 14 MeV neutron source. The neutron multiplier, M_n, which was required to fit this particular data set was 70. The induced absorption spectral shape is similar to that shown in Fig. 5a for the fission reactor induced absorption, indicating that no fundamentally new defects are created. The number of defects per collision is expected to be higher for 14 versus 1 MeV neutrons, however. Data taken on RTNS-II in 1987 by Singh et al. at much higher doses (10^{16} n/cm^2) implied a neutron multiplier of 200. Data taken on LANSCE was roughly consistent with this neutron multiplier range although detailed dosimetry of neutron fluence as a function of the neutron energy for the broad spectrum on LANSCE is still being analyzed. The overall spread of up to a factor of three in neutron damage effectiveness (M_n) is large depending on the experiment. The neutron multiplier that was inferred from these experiments varied over the range of 70 to 200 depending on the dose and neutron source. Perhaps this may be due to neutron dosimetry calibration differences or due to other uncertainties in the radiation environment such as the ratio of neutron to gamma dose. To be conservative we will use M_n = 200 at the upper end of the measured range to predict the NIF performance.

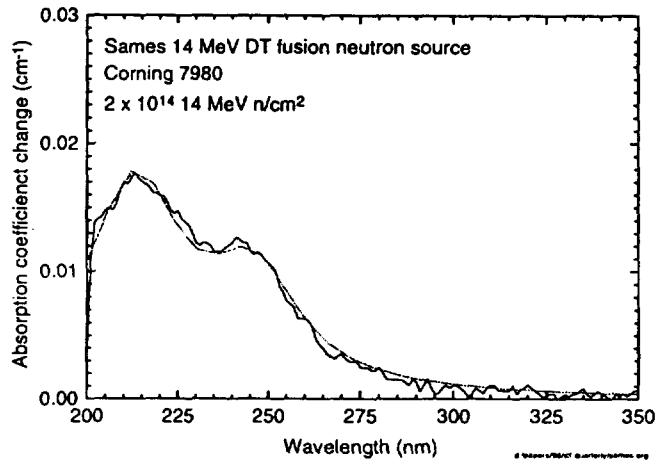

Figure 9. Absorption induced by French CEA Sames 14 MeV DT fusion neutron source with $2x10^{14}$ n/cm^2 fluence at room temperature. Data and theory curves are shown.

B. Predictions for silica glass on NIF

The predicted transmission of silica glass as a function of time on NIF is plotted in Fig. 10, for both type FS1 and fused quartz type FQ1, with an initial condition of $N_{Ce} = 3x10^{16}$ cm^{-3} determined from data. The final focus lens is assumed to be 4.5 cm thick. Thicker lens designs would be expected to have larger absorbance (-log transmission) that is proportional to the thickness. It is apparent from the predictions in Fig. 10 that FS1 fused silica is significantly more radiation resistant than FQ1 fused quartz at 3ω. Fused silica is expected to have >99% transmission over the 30 year facility lifetime. Fused quartz, however is expected to drop to a 99% lens transmission within one year which is undesirable. Fortunately FS1 is the current baseline material that was also assumed in the CDR.

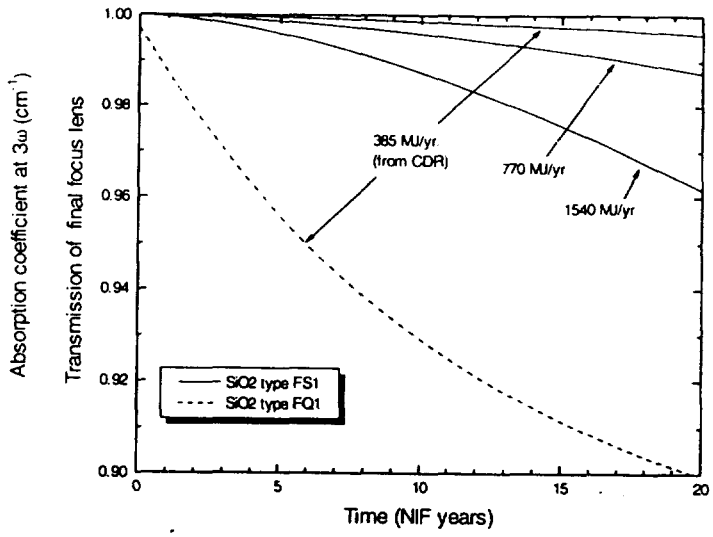

Figure 10 Predicted transmission of NIF final focus lens versus time for fused silica type FS1 such as Corning 7980 or Heraeus Suprasil (solid lines) and fused quartz type FQ1 such as Heraeus Herasil 1-SV (dashed line). Predictions for the NIF CDR fusion yield of 385 MJ/year as well as 2X and 4X that shot rate as shown for fused silica.

If the shot rate or target yields on NIF were increased by 2 to 4 times over that assumed in the NIF CDR, (yield rates of 770 and 1540 MJ/yr.), the lifetime of the silica final focus lenses would be reduced. Figure 10 presents our predictions for these shots rates which lower the effective lifetime to 18 and 9 years for 2X and 4X increase in yield rate, respectively. This would present a incrementally small increase in the NIF operational cost over the 30 year facility lifetime.

C. KDP impurity related radiation effects

The results of irradiation experiments with both γ-rays and neutrons would indicate that only the γ-rays have a measurable impact on the UV transmission spectra of KDP at integrated doses relevant to NIF. In Fig. 11, the spectral results of 2 representative KDP/KD*P crystals are presented for samples irradiated on SPR-III (n° and γ-ray source) and ^{60}Co (γ-ray source only). The spectral features observed after similar γ-ray dose from the two sources, are nearly identical in shape and magnitude, demonstrating that the presence of ~1 MeV n°'s in SPR-III does not produce any observable optical damage in KDP. There will be direct knock-on neutron collisions that will introduce non crystalline defects, however, they do not appear to introduce optically absorbing species. It is noteworthy that no refractive index changes were experimentally observed up to 1 part in 10^5.

The distinction of the different spectra of Fig. 11 appear to correlate to the presence of impurities detected by wet chemical analyses which have been performed on several of the crystals. Most KDP samples give rise to relatively featureless spectra which show a slight overall increase in absorption (< 0.03 cm^{-1} at 3ω). These samples are represented in Fig. 11(a) and (b). The strong absorption band at ~ 263 nm are typical of As containing KDP and KD*P as seen in Figs. 11c and 11d. Other radiation sensitive impurities have also been identified and will be discussed further below.

In the particular case of As, where the readily incorporated $(AsO_4)^{3-}$ substitutes isomorphically for the$(PO_4)^{3-}$ group, irradiation by γ-rays turns the anion complex into a color center with a peak absorption at 263 nm, that is presumably $(AsO_4)^{4-}$ based on some evidence in the literature.[10,11] In order to test the correlation of As with the strongly absorbing peak at ~263 nm, 5 samples were selected for analyses by

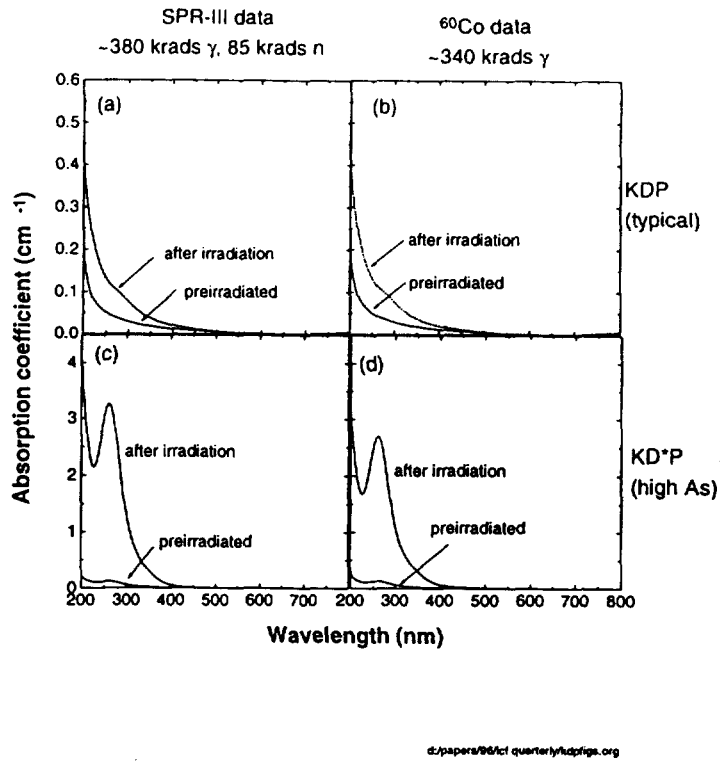

Figure 11. KDP and KD*P spectra before and after irradiation with 380 krads γ-ray and 85 krads neutrons (parts a and c) or 340 krads γ-ray (parts b and d). Note that the spectra are virtually identical with and without the 85 krads neutron dose indicating that γ-ray damage is expected to dominate the radiation effects for NIF KDP/KD*P. The differences between samples types are due to impurities. All spectra are σ-polarized.

the technique of inductively coupled plasma (ICP) mass-spectroscopy. The results in Fig. 12 show the absorption coefficient of the 263 nm peak as a function of the As concentration. In this case, the absorption coefficient was taken from spectra collected after irradiation on SPR-III (for a γ-dose of 380 krads). A linear regression to the data appears to be a good fit indicating that As is responsible for the absorbing defect center.

Since As impurities appear to play the most important role in radiation induced damage in all of the materials studied to date, we have recently completed a study to understand the dose dependence of this phenomena. This study allows for predictions of NIF performance based on the integrated γ-ray dose present in the final optics package as a function of time. Figure 13 presents a compilation of results from the SPR-III pulsed nuclear reactor, the LLNL ^{60}Co continuous γ-ray source, and the LLNL pulsed spallation γ-ray source (LINAC), and the LANL pulsed spallation n" and γ-ray source (LANSCE). All of the data fall onto one curve indicating that the pulse length and radiation spectra do not play a primary role in modifying the radiation induced damage in KDP. This can be rationalized by realizing that γ-rays impart energy to the electronic portion of the atomic structure via Compton scattering. This first

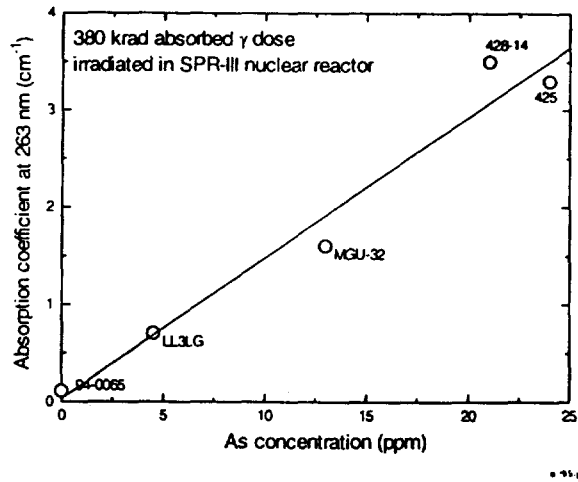

Figure 12. Arsenic concentration in ppm by weight versus 380 krads γ-ray induced σ-polarized absorption coefficient at 263 nm for several KDP and KD*P samples as noted. The good linear correlation suggests that As serves as a precursor for the radiation induced 263 nm absorption.

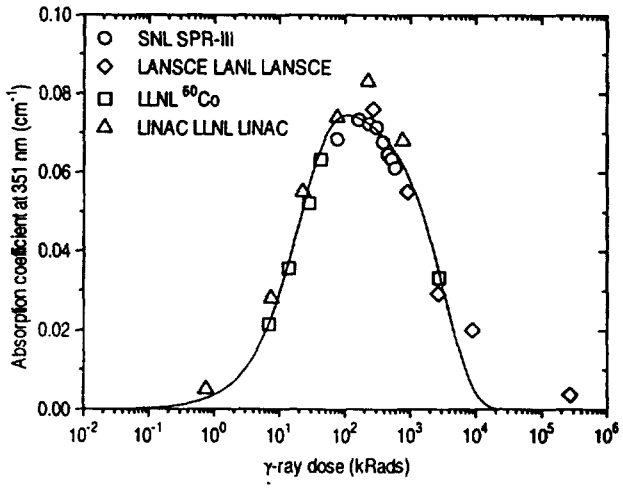

Figure 13. γ-ray induced absorption at 3ω (351 nm) as a function of gamma ray dose. For reference NIF is expected to have 160 krads of for each decade of operation. The independence data from the source characteristics suggests that the total integrated dose, independent of γ-ray spectral or temporal characteristics is adequate for phenomenologically modeling radiation damage in NIF.

produces a ~100 keV electron for each 1 MeV of initial γ-ray energy, that then rapidly scatters via cascade e-e reactions to form multiple ~10 eV electrons. As a consequence, the initial energy of the γ-ray determines the number rather than the damage characteristics of final energetic electrons. These ~10 eV electrons next form defects in the material by trapping at precursor sites (e.g. impurities). This simple mechanism is linearly related to the time-integrated radiation-induced electron density in the conduction band of the material and as a consequence does not depend on the initial γ-ray spectrum or temporal pulse length to first order.

A simple mechanism is proposed based on the As precursors described above where

$$AsO_4^{3-} \xrightarrow{\gamma-rays} AsO_4^{4-} \xrightarrow{\gamma-rays} AsO_3^{2-} + O^{2-}. \quad (8)$$

the second AsO_4^{4-} species causes the 263 nm absorption as shown in Fig. 11c, while the AsO_3^{2-} species is believed to have minimal observable absorption. Initial conditions are determined from the concentration of As in the crystal and all of the As is assumed to be of the form AsO_4^{3-}. A straightforward set of coupled rate equations for the concentration of AsO_4^{3-}, AsO_4^{4-}, and AsO_3^{2-}:O^{2-} leads to an analytic solution for the absorption coefficient at 3ω of the form:

$$\alpha = \frac{A_3^o \sigma_{As} \beta_{32}}{(\beta_{21} - \beta_{32})}\left[\exp(-D'\beta_{32}t) - \exp(-D'\beta_{21}t)\right]. \quad (9)$$

The parameters utilized to fit the data in Fig. 13 using Eq. 9 are defined and quantified in Table IV.

Table IV. Parameters utilized to model data in Fig. 13 and to predict NIF KDP final optics performance in Fig. 14.

Parameter	Value	Units	Source
As concentration in Beamlet KD*P boule (LL3LG), A_3^o	8.3×10^{16}	cm^{-3}	measured
Defect optical absorption cross section, σ_{As}	9.3×10^{-19}	cm^2	data fit
Rate constant for first step in Eq. 4, β_{32}	0.047	1/krad	data fit
Rate constant for second step in Eq. 4, β_{21}	3.0×10^{-5}	1/krad	data fit
Gamma ray dose rate, D'	15.9	krad/yr.	Ref. 1

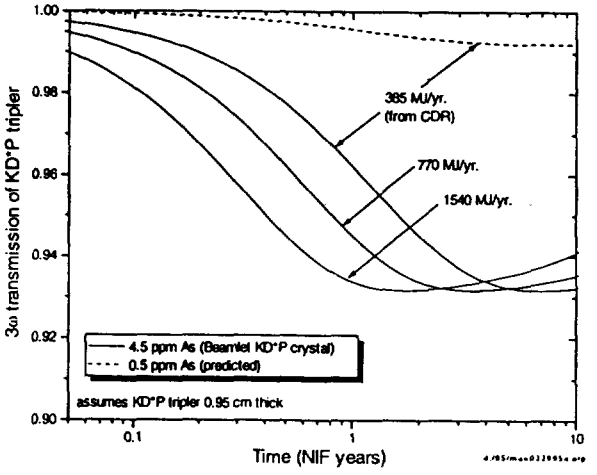

Figure 14. Predicted transmission of NIF KD*P tripler crystal as a function of time for different fusion yield assumptions and levels of As impurities.

Using the data in Table IV one can predict the 3ω transmission of a NIF tripler KD*P crystal, that is taken to be 0.95 cm thick, for different DT fusion yields and As impurity concentrations. Figure 14 gives predictions for three different fusion yield scenarios on NIF ranging from a baseline operation of 385 MJ/year to four times this rate (higher gain per shot and/or higher shot rate) for crystals with the same amount of As as a recent crystalline boule grown for the NIF prototype Beamlet Laser System (4.5 ppm As). It is apparent that in any of these cases the transmission of the tripler drops gradually to 93% within ~1 year. It is clearly undesirable to have this level of loss routinely on NIF following the first year of full yield operation. The dotted line in Fig. 14 shows the predicted transmission of a tripler KD*P crystal for 0.5 ppm As concentration. The transmission of this crystal is expected to exceed 99% for the lifetime of

the facility. Consequently, this is the maximum level of As that would be desirable in NIF KDP triplers. It should be possible to hold the As concentration below this value by utilizing high purity starting materials.[25]

In addition to As impurities in KDP described above, there could be other impurities that cause significant problems in KDP at ppm levels. To test this hypothesis we irradiated 15 KDP crystals with 14 different impurity dopants and one undoped sample. The SPR-III reactor was utilized for these studies and the results are summarized in Table V and Fig. 15. We found that other impurities, most notably transition metals such as Al, Fe, As, Cr, Pb, and V, can lead to significant radiation induced absorption in KDP. We measured the concentrations of all the dopants in the crystals using inductively-coupled-plasma mass spectroscopy, in the growth solution and spectra before and after a dose of $1.4x10^{15}$ n/cm^2 and 473 krads of γ-rays. It is clear that many impurities cause problems, and that it would not be practical to test the entire periodic table. Consequently, we should develop a testing procedure that utilizes a readily available radiation source such as the ^{60}Co source at LLNL and the actual starting materials to grow test pieces to qualify the starting materials prior to growth of large boules.

Table V. Experimental results of deliberately doping KDP with various impurities and irradiating with 1.4e15 n"/cm^2 1 MeV or 84 kRads of neutrons and 473 kRads of γ-rays (Si equivalent). The absorption coefficients are weighted for concentration and were background corrected with a blank sample that showed induced absorptions of 0.0 %/cm and 5.9 %/cm before and after irradiation, respectively.

Impurity	Concentration in growth solution / crystal (ppm by weight)	Peak absorption wavelength (nm)	Concentration weighted absorption at 3ω before irradiation (%/cm/ppm)	Concentration weighted absorption at 3ω after irradiation (%/cm/ppm)
Al	11 / 5	266	2.7	6.6
Fe	10 / 21	<290	2.7	3.1
As	1000 / 18	263	0.2	2.8
Cr	9 / <4	358 & 270	>2	>6
Pb	50 / 10	<230 &268	0.8	1.8
V	10 / 0.9	266	~20	~40
S	250 / 14	266	0.1	0.3
B	250 / <1	266	>7	>7
Si	250 / <1	266	>6	>6
Na	1000 / 15	266	1.1	1.7
Rb	250 / 26	218	0.6	0.6
Ca	250 / 34	266	0.1	0.3
Sr	100 / 0.8	276	0.7	0.7
Ba	100 / 20	266	0.2	0.3

Figure 16 presents typical σ-polarized spectra utilized to obtain the results in Table III. The spectra in part (a) is for a crystal grown with no deliberate doping, and the resulting change in transmission is minimal. Part (b) through (d) are for Al, Cr, and Pb, respectively. Many of the spectra have absorptions peaked at 266 nm both before and after irradiation that look virtually identical to part (b). This transition was observed to be only weakly polarized. Since many different dopants all provide the same absorption spectra, this peak appears to be due to an intrinsic vacancy or F-center in the KDP lattice induced by the

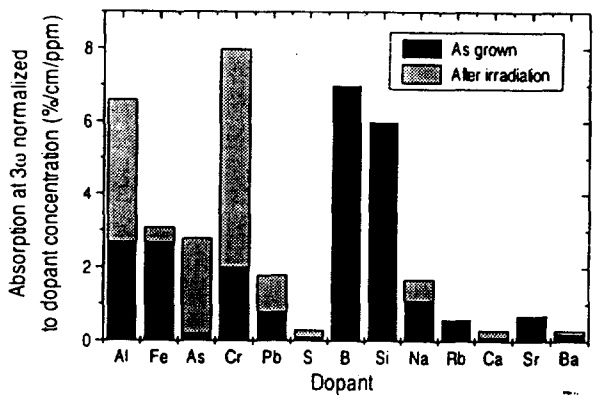

Figure 15. Experimental results of irradiating impurity doped-KDP with 473 krads of γ-rays. The absorption coefficients are weighted for concentration in parts per million by weight (ppm).

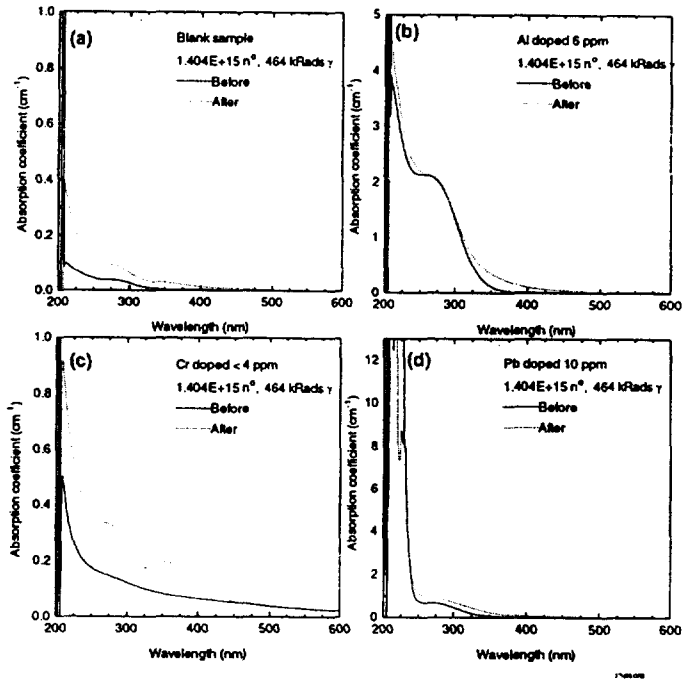

Figure 16. Absorption spectra of KDP with Al, Cr, and Pb, in parts (b) through (d), respectively, before and after irradiation with 1.4×10^{15} neutrons/cm^2 and 473 krads of γ-rays. Part (a) was not intentionally doped and served as a control sample.

presence of a nearby impurity.[26,11] Some of these dopants have measurable increases in 3ω absorption after irradiation. For example, Al-doped KDP appears to initially have ~3%/cm loss, but following I irradiation has ~6%/cm loss due to the peak lowering and broadening as shown in Fig. 16b. This behavior is also observed in general for V, S, B, Si, Na, Rb, Ca, Sr, and Ba dopants although the magnitude of the effect normalized for concentration seems to vary. Other common impurities in KDP are metals such as Fe, Cr, and Pb. These lead to different absorption features, as noted in Table III, with varying degrees of impact on the 3ω transmission. The transition metals also appear to be more sensitive in general to γ-irradiation.

D. High energy neutron irradiation experiments

A remarkable outcome of the experiments described above is lack of absorption in KDP following irradiation with neutron energies of ~1 MeV. The NIF is expected to produce neutrons that are primarily at 14 MeV directly from the DT fusion reaction. Consequently, we have performed experiments at CEA Sames with 14 MeV n irradiation and LANL LANSCE 1-100 MeV n irradiation. Neutron fluxes in these experiments ranged from $2x10^{14}$ n/cm^2 for Sommes to as high as $3x10^{17}$ n/cm^2 on LANSCE. These high energy neutron irradiations agree with the previous 1 MeV SPR-III neutron irradiation results in that there are no observable neutron induced effects in the absorption of the material. Figure 17 shows a typical result for very high purity KDP irradiated to $3x10^{17}$ n/cm^2. This neutron flux is equivalent to ~100 years of operation on NIF at 385 MJ/year thermonuclear yield as assumed in the CDR. The increase in absorption at 3ω is only 5.6 %/cm even after such a large dose. Interestingly there is significantly less change in UV absorption than fused silica which is normally associated with being the "optimal" radiation resistant optical material. As discussed above KDP with impurities can have significantly larger induced absorption.

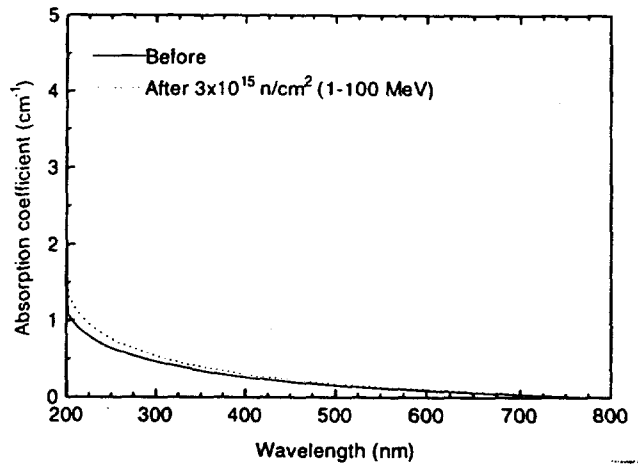

Figure 17. Fast grown KDP sample (LLNL boule LNL-58) before and after irradiation at LANSCE with ns-pulsed 1-100 MeV neutrons and γ-rays with up to ~100 years of NIF dose at CDR shot rates and assumed yields.

This sample serves as an important existence proof that with sufficient purity, KDP can withstand the radiation environment on NIF and have minimal radiation induced absorption losses at 3ω of <1% per decade of NIF yield. There must, of course, be displacements induced in the crystals from direct neutron knock on collisions but they do not appear to manifest themselves optically at doses relevant to NIF. This situation may arise from either the lack of natural color centers capable of near UV or visible absorption as opposed to vacuum UV, or possibly from rapid self-annealing of the local displacements at room temperature. The secondary γ-irradiation that is present appears to induce virtually all of the observed damage in KDP and is consistent with the data reported above.

IV. Summary

We have performed a variety of neutron and gamma ray irradiation experiments in the SNL SPR-III, LANL LANSCE, CEA Sommes, and LLNL's ^{60}Co, and LINAC. These provide complementary sources of γ-rays and neutrons with various energy and pulse formats. Our studies have focused on high-energy penetrating radiation (gamma-rays and neutrons) that will propagate through the debris shield and supply a 3 kRad dose from neutrons and gamma rays to the NIF final optics (final focus lens and frequency conversion crystals) for each 20 MJ equivalent NIF shot. From the experiments and modeling presented, the highest purity fused silica is expected to have <1% loss at 3ω in the final focus lens after 30

years of use at baseline NIF DT fusion yield levels. This optical absorption is due both to neutron induced displacements and γ-ray induced color center formation. Neutrons induce an absorption peak centered at 246 nm while γ-rays introduce absorption peaks centered at 210 nm and 300 nm in high purity fused silica and fused quartz, respectively. Increasing the shot rate or yield by 4X over CDR assumptions is expected to decrease the effective lifetime to 8 years for a ~1% loss level. If fused quartz (such as Heraeus Herasil 1) is utilized, 1% loss levels are reached within 1 year for CDR level fusion yields. Therefore it is advisable that only radiation resistant synthetic fused silica should be utilized for the final focus lenses.

Experiments performed on KDP indicate that neutron collisions do not appear to degrade the optical properties of KDP at NIF relevant fluences and (2) γ-rays can cause significant problems if impurities such as arsenic are present at ppm levels. For As, which appears to be a common impurity, we have been able to construct a physical picture and measure quantitative parameters necessary to model the radiation-induced losses expected for KDP and KD*P. We also found that other impurities such as Al, Fe, As, Cr, Pb, and V can also cause significant problems at ppm level concentrations. Assuming these impurities are brought to acceptable levels, the neutron and gamma ray damage to the KDP arrays should not present a significant problem for >1 decade of operation on NIF. In fact the more pure growths of KDP at LLNL showed virtually no observable degradation (<1%/cm losses) at up to the equivalent dose of up to ~100 NIF years, using the LANSCE facility at LANL that has a more severe radiation environment than that expected on NIF.

V. Acknowledgments

We would like to especially thank M. Borden, S. Sterbenz and W. Sommer of Los Alamos National Laboratory for their experimental efforts and insight at LANSCE and S. Karr, D. Berry and P. Griffin of Sandia National Laboratory for their invaluable efforts in coordinating and performing the SPR-III experiments. At LLNL, we wish to thank C. Orth for discussing the neutronic cross sections with us, M. Tobin and J. Latkowski for calculating the radiation source characteristics, T. Diaz-de-la-Rubia for sharing his insights into the neutronic defect mechanisms, C. Bibeau for assistance with the analytic KDP modeling, and also J. Marion, M. Yan, N. Zaitseva, J. Atherton, J. Campbell, and J. DeYoreo for their interest and guidance. We also thank R. Torres for the ICP-MS work, and T. Cowan for performing and enabling the e⁻ accelerator spallation experiments. We also thank M. Singh for sharing his RTNS-II data taken in 1987 and more recent insights, and R. Vallene and P. Thelin for sample fabrication.

VI. References

[1]W. A. Bookless and D. Wheatcraft, Report No. UCRL-52000-94-12, 1994.

[2]C. D. Orth, S. A. Payne, and W. F. Krupke, "A diode pumped solid state laser driver for inertial fusion energy," Nuclear Fusion **36** (1), 75-115 (1996).

[3]A. Smakula, J. Opt. Soc. Am. **40**, 266 (1950).

[4]R. A. Weeks and C. Nelson, J. Am. Ceram. Soc. **43**, 399 (1960).

[5]D. L. Griscom, J. Ceram. Soc. Jpn. **99**, 923 (1991).

[6]D. L. Griscom, SPIE **541**, 38 (1986).

[7]M. Rothschild and D. J. Ehrlich, J. Vac. Sci. Technol. B **6**, 1 (1988).

[8]M. Rothschild, R. B. Goodman, M. A. Hartney *et al.*, J. Vac. Sci. Technol. B **10**, 2989 (1992).

[9]D. J. Krajnovich, I. K. Plour, A. C. Tam *et al.*, SPIE Proceedings **1848**, 544 (1992).

[10]A. N. Levchenki, V. M. Shulga, and A. O. Doroshenko, "Impurity origin of of the optical absorption and luminescence spectra of irradiated KDP crystals," Sov. Phys. Solid State **32**, 1432 (1990).

[11]G. N. Pirogova, Y. V. Coronin, V. E. Kritskaya *et al.*, "Effect of radiation on the optical properties of some ferroelectrics," Inog. Materials 22, 97 (1986).

[12]C. D. Marshall, J. A. Speth, and S. A. Payne, "Induced optical absorption in gamma and neutron irradiated fused quartz and silica," J. Non-Crystalline Solids in press (1996).

[13]E. U. Condon and H. Odishaw, *Handbook of Physics* (McGraw-Hill, New York, 1967).

[14]D. H. Levy, K. K. Gleason, M. Rothschild *et al.*, Appl. Phys. Lett. 60, 1667 (1992).

[15]M. Guzzi, M. Martini, A. Paleari *et al.*, J. Phys. Condens. Matt. 5, 8105 (1993).

[16]H. Imai, K. Arai, J. Isoya *et al.*, Phys. Rev. B 44, 4812 (1991).

[17]R. A. Weeks, J. Non-Cryst. Solids 179, 1 (1994).

[18]R. A. Weeks, J. Am. Ceram. Soc. 53, 176 (1970).

[19]J. Latkowski, , 1995.

[20]G. A. Zawadzkas, P. A. Kuenstler, and L. M. Choate, Report No. SAND83-0598, 1985.

[21]T. Diaz-de-la-Rubia and W. J. Phythian, J. Nucl. Materials 191, 108 (1992).

[22]M. S. Livingston and J. P. Blewet, *Particle Accelerators* (McGraw-Hill, New York, 1962).

[23]J. Wong, T. Diaz-de-la-Rubia, M. W. Guinan *et al.*, J. Nucl. Material 212, 143 (1994).

[24]T. Diaz-de-la-Rubia, M. W. Guinan, A. Caro *et al.*, Rad. Effects in Solids 130, 39 (1994).

[25]J. Atherton and J. DeYoreo (personal communication).

[26]M. Yang (personal communication).

This work was performed under the auspices of the U.S. Department of Energy by Lawrence Livermore National Laboratory under contract No. W-7405-Eng-48.

Technical Information Department • **Lawrence Livermore National Laboratory**
University of California • Livermore, California 94551